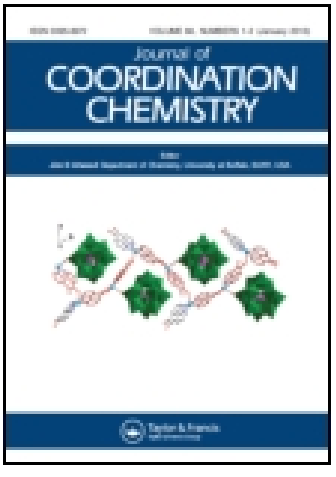

Journal of Coordination Chemistry
Publication details, including instructions for authors and subscription information:
http://www.tandfonline.com/loi/gcoo20

Synthesis, structural characterization, molecular docking, and urease inhibition studies of dinuclear cobalt(II) complexes derived from 3,5-bis(pyridin-2-yl)-4-amino-1,2,4-triazole

Jie Qin[a], Na Lei[a] & Hai-Liang Zhu[a]
[a] School of Life Sciences, Shandong University of Technology, Zibo, PR China

Accepted author version posted online: 27 Mar 2014.Published online: 22 Apr 2014.

To cite this article: Jie Qin, Na Lei & Hai-Liang Zhu (2014) Synthesis, structural characterization, molecular docking, and urease inhibition studies of dinuclear cobalt(II) complexes derived from 3,5-bis(pyridin-2-yl)-4-amino-1,2,4-triazole, Journal of Coordination Chemistry, 67:7, 1279-1289, DOI: 10.1080/00958972.2014.909591

To link to this article: http://dx.doi.org/10.1080/00958972.2014.909591

Journal of Coordination Chemistry, 2014
Vol. 67, No. 7, 1279–1289, http://dx.doi.org/10.1080/00958972.2014.909591

Synthesis, structural characterization, molecular docking, and urease inhibition studies of dinuclear cobalt(II) complexes derived from 3,5-bis(pyridin-2-yl)-4-amino-1,2,4-triazole

JIE QIN*, NA LEI and HAI-LIANG ZHU

School of Life Sciences, Shandong University of Technology, Zibo, PR China

(*Received 7 January 2014; accepted 17 March 2014*)

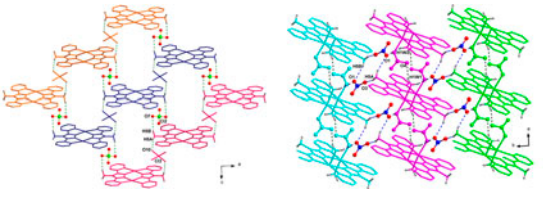

Two dinuclear Co(II) complexes, $[Co_2(\mathbf{L})_2(EtOH)_4]\cdot 4ClO_4$ (**1**) and $[Co_2(\mathbf{L})_2(H_2O)_2(NO_3)_2]\cdot 2NO_3$ (**2**) (**L** = 4-amino-3,5-bis(pyridin-2-yl)-1,2,4-triazole), have been obtained and characterized by IR, elemental analysis, and single-crystal X-ray diffraction analysis. The stabilization of their crystal lattices is maintained by strong H-bonds between counterions and host framework, which lead to various supramolecular architectures. The urease inhibitory properties of **1**, **2**, and **L** were investigated, where the two complexes revealed strong urease inhibition activities. Docking simulations of **2** have been performed with H. pylori urease (PDB code: 1E9Z) to rationalize their binding models.

Keywords: Dinuclear cobalt complexes; Crystal structures; Urease inhibitors; Molecular docking

1. Introduction

Urease (urea amidohydrolase EC 3.5.15), a nickel-containing metalloenzyme, can catalyze the hydrolysis of urea to form ammonia and carbamate [1]. High concentration of ammonia arising from the reaction, as well as the accompanying abrupt pH elevation, has marked negative impacts on plants and animals [2–7]. Therefore, it is important to control the activity of urease through the use of inhibitors.

*Corresponding author. Email: qinjietutu@163.com

Although many urease inhibitors, including organic molecules such as hydroxamic acids, phosphoramides, thiols, and metal ions have been reported [8–12], much effort has been devoted to find more efficient inhibitors owing to the low efficiency and negative side effects of the presently available inhibitors. Considerable attention has been paid to biologically active metal complexes as potential urease inhibitors [13, 14]. On coordination, bioactive ligands may improve their bioactivity profiles and inactive ligands may acquire pharmacological properties [15, 16]. Coordination can cause the slow release of metal ions, which is advantageous in reducing toxic side effects. Reported urease inhibition complexes are based on Schiff bases or cinnamic acid derivatives [14, 17–20]. These complexes show enhanced inhibitory activities compared to parent ligands, due to these complex molecules being well filled in the active pocket of the urease, and interactions have been established between complexes and the active site of the urease.

We are focusing on designing and synthesizing urease inhibitors based on triazole complexes. Triazoles, a versatile group of heterocycles, are known chemotherapeutic agents possessing potential urease inhibition [21, 22] and are capable of forming complexes with metal ions. Two new dinuclear cobalt(II) complexes with 4-amino-3,5-bis(pyridin-2-yl)-1,2,4-triazole (**L**), $[Co_2(\mathbf{L})_2(CH_3CH_2OH)_4]\cdot 4ClO_4$ (**1**), and $[Co_2(\mathbf{L})_2(H_2O)_2(NO_3)_2]\cdot 2NO_3$ (**2**) were synthesized (scheme 1) and structurally characterized. The urease inhibitory activities of the complexes were investigated from both experimental and molecular docking study.

2. Experimental

2.1. *Materials and measurements*

Unless otherwise stated, all solvents were of reagent grade and purchased commercially. All chemicals were also commercially available and used without purification. 4-Amino-3,5-bis (pyridin-2-yl)-1,2,4-triazole (**L**) was synthesized according to the literature procedure [23, 24]. IR spectra were recorded on a FT-IR Nicolet 5700 spectrometer from 4000 to 400 cm^{-1} with KBr pellets. Elemental analyses for C, H, and N were performed on a Perkin-Elmer 240C analyzer.

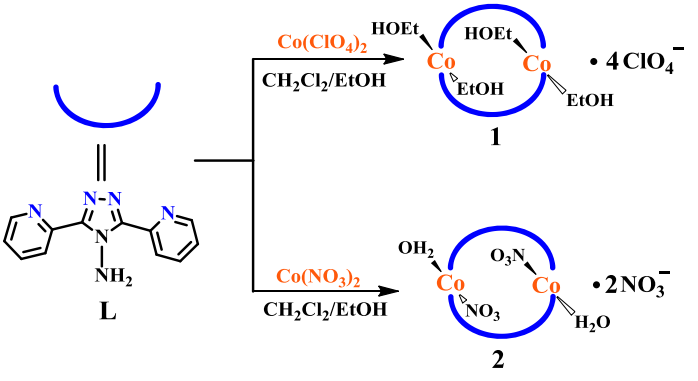

Scheme 1. Synthetic routes to **1** and **2**.

2.2. *Synthesis of $[Co_2(L)_2(CH_3CH_2OH)_4]\cdot 4ClO_4$ (1)*

$Co(ClO_4)_2$ (0.08 mM) in ethanol solution (4 mL) was carefully layered on top of dichloromethane solution (4 mL) of **L** (0.08 mM). The solutions were left for 2 days at room temperature and orange crystals were obtained. Yield: 66%, IR (KBr, cm^{-1}): 3318, 1635, 1608, 1591, 1537, 1496, 1459, 1428, 1297, 1258, 1114, 1099, 1090, 1016, 795, 749, 703, 628, 424. Anal. Calcd for $C_{32}H_{44}Cl_4N_{12}O_{20}Co_2$ (%): C, 32.67; H, 3.77; N, 14.29. Found: C, 32.75; H, 3.76; N, 14.31.

2.3. *Synthesis of $[Co_2(L)_2(H_2O)_2(NO_3)_2]\cdot 2NO_3$ (2)*

Complex **2** was obtained with similar procedure as for **1** by using $Co(NO_3)_2$ instead of $Co(ClO_4)_2$. Yield: 73%, IR (KBr, cm^{-1}): 3283, 1637, 1607, 1494, 1459, 1384, 1309, 1155, 1093, 1025, 827, 795, 749, 701, 638, 607, 418. Anal. Calcd for $C_{24}H_{24}N_{16}O_{14}Co_2$ (%): C, 32.82; H, 2.75; N, 25.51. Found: C, 32.88; H, 2.73; N, 25.56.

2.4. *X-ray crystallography*

The data were collected on a Bruker Smart Apex CCD diffractometer equipped with graphite-monochromated Mo Kα ($\lambda = 0.71073$ Å) radiation using a $\omega - 2\theta$ scan mode at 293 K. The collected data were reduced using SAINT [25] and multi-scan absorption corrections were performed using SADABS [26]. The structures were solved by direct methods and refined against F^2 by full-matrix least-squares using SHELXTL [27]. All non-hydrogen atoms were found in alternating difference Fourier syntheses and least-squares refinement cycles and, during the final cycles, refined anisotropically. All hydrogens bonded to C were generated geometrically and refined isotropically using the riding model. Hydrogens bound to N or O were first found in the Fourier map and then fixed at their ideal positions. Hydroxyl of EtOH were refined with distance restraints of O–H = 0.92(2) Å and *Uiso*(H) = 1.5*Ueq*(O). Water H were refined with distance restraints of O–H = 0.85(2) Å, H···H = 1.44(2) Å, and *Uiso*(H) = 1.5*Ueq*(O). Amino H were refined with distance restraints of N–H = 0.83(2) Å, H···H = 1.30(2) Å, and *Uiso*(H) = 1.5*Ueq*(N).

2.5. *Measurement of inhibitory activity against jack bean urease*

Jack bean urease was purchased from Sigma Aldrich Co. (St. Louis, MO, USA). The measurement of urease was carried out according to the literature [28, 29]. Generally, the assay mixture, containing 25 mL of jack bean urease (10 kU^{-1} L) and 25 mL of the tested complexes of various concentrations [dissolved in DMSO : H_2O = 1 : 1 (v : v)], was preincubated for 1 h at 37 °C in a 96-well assay plate. After preincubation, 0.2 mL of 100 mM HEPES (N-[2-hydroxy-ethyl]piperazine-N′-[2-ethanesulfonic acid]) buffer pH 6.8 containing 500 mM urea and 0.002% phenol red was added and incubated at 37 °C [30]. The reaction time was measured by microplate reader (570 nm), which was required to produce enough ammonium carbonate to raise the pH of a HEPES buffer from 6.8 to 7.7, the endpoint being determined by the color of phenol red indicator [31]. The abilities of the ligand, 4-amino-3,5-bis(pyridin-2-yl)-1,2,4-triazole, and complexes **1** and **2** as inhibitors were studied by the inhibition rate values of the material (25 mL, 100 mg) tested against jack bean urease (25 mL, 10 kU^{-1} L) using urea (500 mM) in HEPES buffer (0.2 mL, 100 mM; pH 6.8).

2.6. *Docking study*

The automated docking studies were carried out using AutoDock version 4.2. First, the AutoGrid component of the program precalculates a 3-D grid of interaction energies based on the macromolecular target using the AMBER force field. A cubic grid box of 62 Å size (x, y, z) with a spacing of 0.375 Å for mode A (85 Å for mode B) and grid maps were created representing the catalytic active target site region where the native ligand was embedded. Then, automated docking studies were carried out to evaluate the binding free energy of the inhibitor within the macromolecules. The GALS search algorithm (genetic algorithm with local search) was chosen to search for the best conformers. The parameters were set using the software ADT (AutoDockTools package, version 1.5.4) on a PC, which is associated with AutoDock 4.2. Default settings were used with an initial population of 50 randomly placed individuals, a maximum number of 2.5×10^6 energy evaluations, and a maximum number of 2.7×10^4 generations. A mutation rate of 0.02 and a crossover rate of 0.8 were chosen. Results differing by less than 0.5 Å in positional root-mean-square deviation were clustered together and the results of the most favorable free energy of binding were selected as the resultant complex structures.

3. Results and discussion

3.1. *Synthesis*

L was synthesized by a one-pot procedure. Dinuclear **1** and **2** were obtained by coordination of **L** with Co(II) salts. In these specific reactions, the products do not depend on the ligand-to-metal ratio.

3.2. *IR spectra*

The IR spectra of **L**, **1,** and **2** are depicted in figure 1. **L** displays typical NH_2 stretch at 3295 cm^{-1}; for **1** and **2**, the medium broadbands at 3420–3080 cm^{-1} are attributed to overlapped NH_2 and O–H stretches. The main spectral variations between complexes and free ligand are in the regions of pyridine ring vibrations [32]. Compared with free ligand, the pyridine ring stretches for **1** and **2** are shifted to higher wavenumbers (1588 cm^{-1} for **L**, 1608 cm^{-1} and 1607 cm^{-1} for **1** and **2**, respectively). The pyridine ring deformations for **1** and **2** are also shifted to higher wavenumbers (587 and 404 cm^{-1} for **L**, 424 cm^{-1} for **1**, and 607 and 418 cm^{-1} for **2**). These variations suggest coordination of N_{py} to Co(II). Slightly lower frequency shifts in ν(C=N) of the triazole ring suggest coordination of $N_{triazole}$. The sharp absorption bands of ClO_4^- for **1** are clearly visible at 1099 and 628 cm^{-1} while the NO_3^- stretching bands in **2** are at 1384 and 827 cm^{-1}.

3.3. *Crystal structure description*

The solid structures of **1** and **2** were determined by single-crystal X-ray diffraction. The crystallographic and data collection parameters are given in table 1; selected bond lengths and angles are listed in tables 2 and 3.

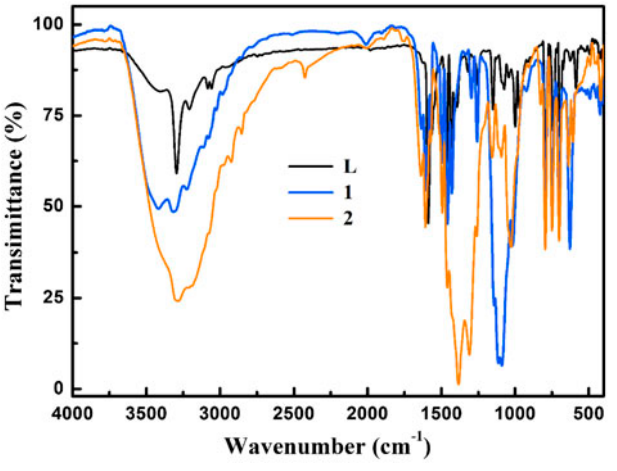

Figure 1. IR spectra of **L**, **1**, and **2**.

Table 1. Crystallographic data for **1** and **2**.

	1	**2**
Empirical formula	$C_{32}H_{44}Cl_4Co_2N_{12}O_{20}$	$C_{24}H_{24}Co_2N_{16}O_{14}$
M_r	1176.45	878.45
Cryst. syst.	Monoclinic	Triclinic
Space group	*C2/c*	*P-1*
a (Å)	16.9082(7)	7.7390(1)
b (Å)	21.0229(1)	10.1564(1)
c (Å)	13.3146(6)	11.4124(2)
α (°)	90.00	72.94(4)
β (°)	90.87(2)	76.71(4)
γ (°)	90.00	87.21(4)
V (Å^3)	4732.3(4)	834.4(2)
Z	4	1
ρ_c (g cm^{-3})	1.651	1.748
F(0 0 0)	2408	446
T (K)	293(2)	293(2)
μ(Mo Kα) (mm^{-1})	1.015	1.088
GOF (F^2)	1.034	1.032
R_1[a], wR_2[b] ($I > 2\sigma(I)$)	0.0615, 0.1659	0.0450, 0.1072

[a] $R_1 = \Sigma||C| - |F_c||/\Sigma F_o|$.
[b] $wR_2 = [\Sigma w(F_o^2 - F_c^2)^2/\Sigma w(F_o^2)]^{1/2}$.

Complex **1** crystallized in the monoclinic space group *C2/c*. As shown in figure 2, **L** is bis-bidentate, bridging Co(II) ions forming dimeric structure of **1**. The Co(II) is in a pseudo-octahedral environment with four nitrogens (N1, N2, N3, and N6) in the equatorial plane. The Co–$N_{triazole}$ bond lengths (2.071(14) and 2.075(13) Å) are shorter than Co–N_{py} distances (2.190(14) and 2.213(13) Å) (table 2). The axial positions are occupied by two ethanol molecules with an average Co–O bond length of 2.084 Å. The bond angle of O(2)–Co(1)–O(1), 170.0(1)°, indicates that the three atoms are in an almost linear configuration. The Co···Co distance is 4.21(1) Å, within the normal range described in dinuclear cobalt(II) complexes, $[Co_2(\mathbf{pldpt})_2(DMF)_2(H_2O)_2](ClO_4)_4{\cdot}0.5Et_2O$ (pldpt = 3,5-di(2-pyridyl)-4-(1H-pyrrol-1-yl)

Table 2. Selected bond distances (Å) and angles (°) for **1**.

Co(1)–N(1)	2.190(14)	Co(1)–N(2)	2.071(14)
Co(1)–N(3)	2.075(13)	Co(1)–N(6)	2.213(13)
Co(1)–O(1)	2.075(13)	Co(1)–O(2)	2.093(14)
N(2)–Co(1)–N(3)	93.09(3)	N(2)–Co(1)–O(1)	94.08(15)
N(3)–Co(1)–O(1)	94.27(14)	N(2)–Co(1)–O(2)	79.69(11)
N(3)–Co(1)–O(2)	97.04(15)	O(1)–Co(1)–O(2)	166.96(6)
N(2)–Co(1)–N(1)	75.18(14)	N(3)–Co(1)–N(1)	168.23(4)
O(1)–Co(1)–N(1)	85.84(13)	O(2)–Co(1)–N(1)	84.40(15)
N(2)–Co(1)–N(6)	166.86(2)	N(3)–Co(1)–N(6)	74.28(12)
O(1)–Co(1)–N(6)	90.54(3)	O(2)–Co(1)–N(6)	86.33(14)
N(1)–Co(1)–N(6)	117.49(3)		

Table 3. Selected bond distances (Å) and angles (°) for **2**.

Co(1)–N(1)	2.192(2)	Co(1)–N(2)	2.073(2)
Co(1)–N(3)	2.065(2)	Co(1)–N(6)	2.211(2)
Co(1)–O(1W)	2.051(2)	Co(1)–O(6)	2.080(2)
O(1W)–Co(1)–N(3)	93.26(9)	O(1W)–Co(1)–N(2)	90.53(9)
N(3)–Co(1)–N(2)	94.86(9)	O(1W)–Co(1)–O(6)	168.14(1)
N(3)–Co(1)–O(6)	90.24(10)	N(2)–Co(1)–O(6)	100.47(1)
O(1W)–Co(1)–N(1)	88.66(9)	N(3)–Co(1)–N(1)	169.33(9)
N(2)–Co(1)–N(1)	74.61(9)	O(6)–Co(1)–N(1)	89.99(1)
O(1W)–Co(1)–N(6)	88.60(9)	N(3)–Co(1)–N(6)	74.29(9)
N(3)–Co(1)–N(6)	74.29(9)	N(2)–Co(1)–N(6)	169.04(9)
O(6)–Co(1)–N(6)	81.44(9)	N(1)–Co(1)–N(6)	116.28(9)
N(8)–O(6)–Co(1)	128.5(12)		

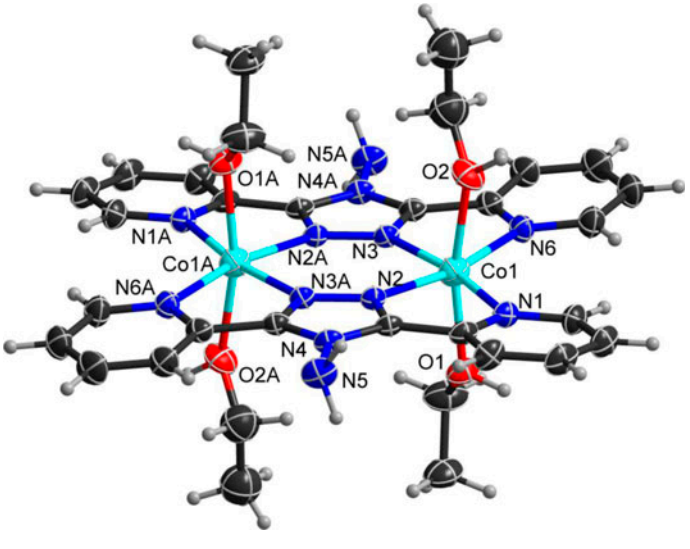

Figure 2. Molecular structure of **1** at 50% probability displacement. Counter anions are omitted for charity.

4H-1,2,4-triazole) with Co···Co distance of 4.27(1) Å [33], and $[Co_2(\mathbf{bpt})_2(SCN)_2(MeOH)_2]$ (bpt = 3,5-di-2-pyridyl-1,2,4-triazolato) with Co···Co distance of 4.19(1) Å [34].

The dinuclear cationic unit is approximately planar except that the amino groups lie out of the plane. The dihedral angle between the chelating plane (containing N3, N6, and Co1) and the coordination plane (containing N1A, N2A, and Co1A) is only 3.9(1)°. Given the strong hydrogen-bonding capability of the uncoordinated $-NH_2$ and ClO_4^- groups, it is not surprising that **1** displays a rigid hydrogen-bonding framework. In the solid state, adjacent dinuclear cationic units are twisted, inclined by 45.8(1)° relative to the central $[Co_2N_4]$ coordination plane. The first kind of ClO_4^- (involving Cl3) are hydrogen bond acceptors and link these dinuclear units into 1-D chain-like structures via N5–H5A···O10 (symmetry code: $-x+3/2$, $-y+1/2$, $-z$). Such 1-D chains are aligned side by side in the *ac* plane and are held together through hydrogen-bonding interactions between the second kind of ClO_4^- (involving Cl2) and $-NH_2$ (N5–H5B···O7, symmetry code: $x+1/2$, $-y+1/2$, $z-1/2$) (figure 3).

These 2-D supramolecular layers are stacked in an –AA– fashion along the crystallographic *b* axis. Several sets of interlayer O–H···O hydrogen bonds have been found in **1**, which consist of O3 and O5 of the ClO_4^- (involving Cl1) and hydrogens H1A and H2A of coordinated ethanol, eventually forming the 3-D network of **1** (figure 4). Therefore, ClO_4^- plays an important role in constructing the supramolecular network.

Crystallization of **L** with $Co(NO_3)_2$ in the same CH_2Cl_2/EtOH solvent system afforded salmon-colored crystals of **2** in 73% yield. Unlike **1**, **2** crystallized in the triclinic space group $P\bar{1}$. An ORTEP view of **2** together with atom numbering scheme is given in figure 5. The double-bridging coordination mode of **L** is also featured in **2**, in which each Co(II) center binds one H_2O and one NO_3^- in the axial positions resulting in distorted octahedral $[N_4O_2]$ coordination. The longer $Co–N_{py}$ distances than $Co–N_{triazole}$ distances are also observed in **2**. The two cobalt centers are 4.16(1) Å apart, which is slightly shorter than that observed in **1**.

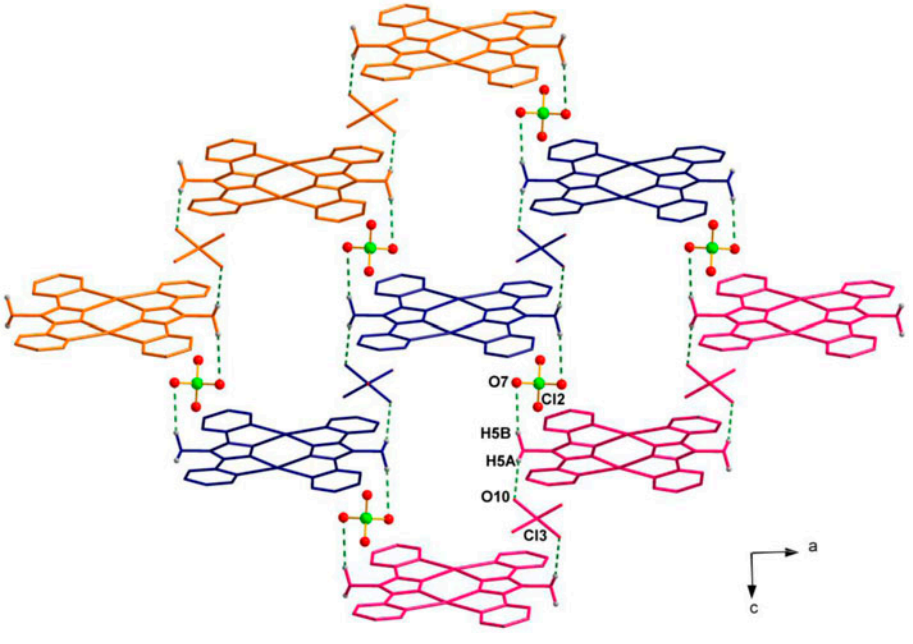

Figure 3. The H-bond-driven 2-D sheet extended in the crystallographic *ac* plane in **1**.

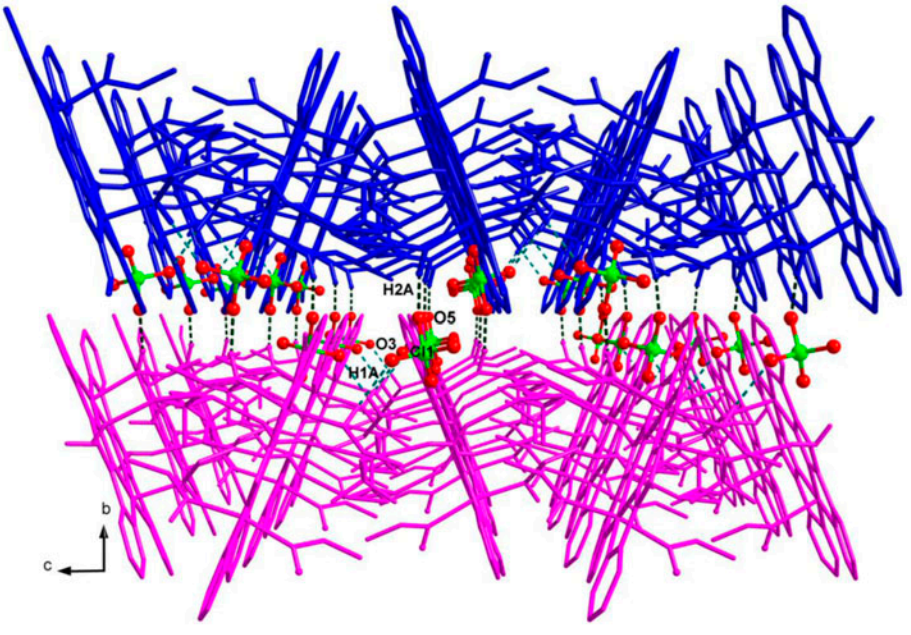

Figure 4. A perspective view of the 3-D hydrogen-bonded network of **1**.

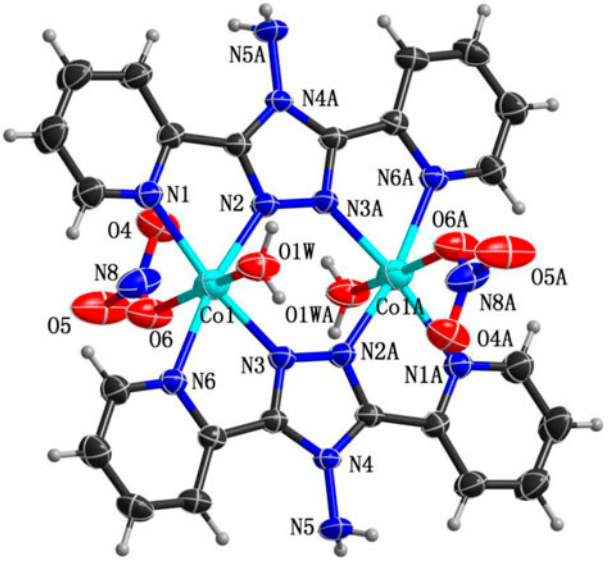

Figure 5. ORTEP drawing of **2** at 50% probability displacement. Counter anions are omitted for clarity.

In the solid state, adjacent dinuclear cationic units of **2** are almost completely coplanar which is different from **1**. The monodentate nitrates are located above or below the dinuclear plane and hold these units into 1-D chains extending along the crystallographic *a* axis

through hydrogen-bonding interactions with coordinated water (O1W–H1W1···O4, symmetry code: $x+1$, y, z). As shown in figure 6, the free nitrates are located between these chains and link them into a 2-D architecture by three sets of hydrogen bonding interactions (O1W–H1W2···O1, N5–H5A···O3$^{\#1}$, and N5–H5B···O1$^{\#2}$; symmetry code: #1: x, $y+1$, $z-1$; #2: $-x+2$, $-y+1$, $-z$).

3.4. *Inhibitory activity against jack bean urease*

In this study, **L**, **1**, and **2** were evaluated for inhibitory activity against jack bean urease. The results are summarized in table 4. From the results, **L** exhibits no ability to inhibit jack bean urease. The percents of inhibition at the concentration of 100 uM for **1** and **2** against urease are 87.8 and 89.9, respectively. The acetohydroxamic acid (AHA) is used as a standard inhibitor with the percent of inhibition of 60.2 at 100 μM. Thus, **1** and **2** possess effective inhibitory activity against jack bean urease with IC_{50} values of 4.62 and 5.51 μM, respectively, which are superior to the positive control AHA ($IC_{50} = 7.21$ μM). The urease inhibitory efficiency of metal ions follows the order: $Cu^{2+} > Ni^{2+} > Co^{2+} > Zn^{2+}$ [35, 36] and complexes possessing strong urease inhibition based on Schiff bases or cinnamic acid derivatives reported before were mostly copper or nickel complexes [18–20]. Our cobalt complexes show inhibitory activities comparable to those of copper or nickel complexes.

3.5. *Molecular docking*

In order to explain the inhibitory activity of the complexes against urease, molecular docking study of the more active **2** in the active sites of urease enzyme from H. pylori urease

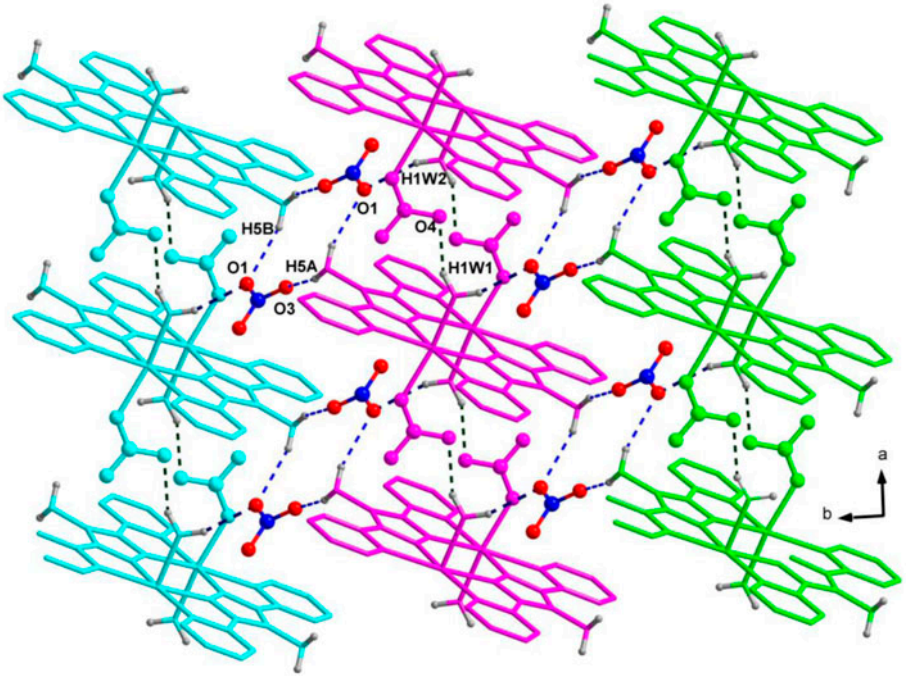

Figure 6. The H-bond-driven 2-D sheet extended in the crystallographic *ab* plane in **2**.

Table 4. Inhibition of jack bean urease by **L**, **1**, and **2**.

Tested materials	IC_{50} (μM)
1	4.63
2	5.51
L	>50
AHA	7.52

Figure 7. The 3-D model structure of **2** binding with **1E9Z**.

(entry 1E9Z in the Protein Data Bank) was carried out by the AutoDock program. The binding mode of **2** with urease enzyme and the enzyme surface model is shown in figure 7. The binding models reveal that the uncoordinated amino groups of **2** form hydrogen bonds with the amino group of HIS322 and ASP223 of the urease with hydrogen-bonding distance of 2.23 Å ($N_{complex}$…H–N_{HIS322}) and 2.14 Å ($N_{complex}$…H–N_{ASP223}), respectively. Polar interaction exists between the benzene ring and the same amino acid (HIS322 and ASP223).

4. Conclusion

In this article, we reported two new Co(II) complexes based on 4-amino-3,5-bis(pyridin-2-yl) 1,2,4-triazole, including the synthesis, characterization, molecular docking, and inhibitory activity against jack bean urease. X-ray crystallographic analysis reveals that these complexes have dinuclear structures and counterions have a profound effect on the resultant supramolecular network. The two complexes have effective inhibitory activity against jack bean urease. Molecular modeling provided further insight into interactions between the enzyme and the complexes. This research showed that metal complexes generated from triazole are potential inhibitors against urease. Detailed investigations are continuing to study the mechanisms of the inhibitory activity against jack bean urease reported here.

Supplementary material

Crystallographic data (excluding structure factors) for the structural analysis have been deposited with the Cambridge Crystallographic Data Center as supplementary publication Nos. CCDC 979617 (**1**) and 979618 (**2**). Copies of the data can be obtained free of charge via www.ccdc.ac.uk/conts/retrieving.html (or from The Director, CCDC, 12 Union Road, Cambridge CB2 1EZ, UK, Fax: +44-1223-336-033; E-mail: deposit@ccdc.cam.ac.uk).

Funding

This work was supported by the National Natural Science Foundation of China [grant number 21301108].

References

[1] P.A. Karplus, M.A. Pearson, R.P. Hausinger. *Acc. Chem. Res.*, **30**, 330 (1997).
[2] H.L.T. Mobley, M.D. Island, R.P. Hausinger. *Microbiol. Rev.*, **59**, 451 (1995).
[3] M. Zaman, J.D. Blennerhassett. *Agric. Ecosyst. Environ.*, **136**, 236 (2010).
[4] B. Krajewska, R. Eldik, M. Brindell. *J. Biol. Inorg. Chem.*, **17**, 1123 (2012).
[5] Z.L. You, D.H. Shi, J.C. Zhang, Y.P. Ma, C. Wang, K. Li. *Inorg. Chim. Acta*, **384**, 54 (2012).
[6] B. Krajewska, R. Eldik, M. Brindell. *J. Biol. Inorg. Chem.*, **17**, 1123 (2012).
[7] A. Sanz-Cobena, L. Sánchez-Martín, L. García-Torres, A. Vallejo. *Agric. Ecosyst. Environ.*, **149**, 64 (2012).
[8] B. Krajewska. *J. Mol. Catal. B Enzym.*, **59**, 9 (2009).
[9] S. Vassiliou, P. Kosikowska, A. Grabowiecka, A. Yiotakis, P. Kafarski, Ł. Berlicki. *J. Med. Chem.*, **53**, 5597 (2010).
[10] M. Font, M.J. Domínguez, C. Sanmartín, J.A. Palop, S. San-Francisco, O. Urrutia, F. Houdusse, J.M. García-Mina. *J. Agric. Food Chem.*, **56**, 8451 (2008).
[11] W.H.R. Shaw. *J. Am. Chem. Soc.*, **76**, 2160 (1954).
[12] X.W. Dong, Y.G. Li, Z.W. Li, Y.M. Cui, H.L. Zhu. *J. Inorg. Biochem.*, **108**, 22 (2012).
[13] A.Y. Louie, T.J. Meade. *Chem. Rev.*, **99**, 2711 (1999).
[14] Z.L. You, L.L. Ni, D.H. Shi, S. Bai. *Eur. J. Med. Chem.*, **45**, 5200 (2010).
[15] D. Senthil Raja, N.S.P. Bhuvanesh, K. Natarajan. *Eur. J. Med. Chem.*, **47**, 73 (2012).
[16] V. Milacic, Q.P. Dou. *Coord. Chem. Rev.*, **253**, 1649 (2009).
[17] Z.L. You, H. Sun, B.W. Ding, Y.P. Ma, M. Zhang, D.M. Xian. *J. Coord. Chem.*, **64**, 3510 (2011).
[18] X.Y. Qiu, J. Wang, D.H. Shi, S.Z. Li, F.L. Zhang, F.Q. Zhang, G.X. Cao, B. Zhai. *J. Coord. Chem.*, **66**, 1616 (2013).
[19] Z.M. Yang, H. Zhu, J. Sun, S.S. Qian, M.N. Cai, H.L. Zhu. *J. Coord. Chem.*, **66**, 2736 (2013).
[20] H. Zhu, Z.Z. Wang, B. Qi, T. Huang, H.L. Zhu. *J. Coord. Chem.*, **66**, 2980 (2013).
[21] M. Hanif, M. Saleem, M.T. Hussain, N.H. Rama. *J. Braz. Chem. Soc.*, **23**, 854 (2012).
[22] I. Khan, S. Ali, S. Hameed, N.H. Rama. *Eur. J. Med. Chem.*, **45**, 5200 (2010).
[23] J.F. Geldard, F. Lions. *J. Org. Chem.*, **30**, 318 (1965).
[24] Y.B. Dong, H.Y. Wang, J.P. Ma, R.Q. Huang, M.D. Smith. *Cryst. Growth Des.*, **5**, 789 (2005).
[25] Bruker. *SMART and SAINT*, Bruker AXS Inc., Madison, WI, USA (2002).
[26] G.M. Sheldrick. *SADABS, Program for Empirical Absorption Correction of Area Detector*, University of Göttingen, Germany (1996).
[27] G.M. Sheldrick. *Acta Crystallogr., Sect. A: Found. Crystallogr.*, **64**, 112 (2008).
[28] T. Tanaka, M. Kawase, S. Tani. *Life Sci.*, **73**, 2985 (2003).
[29] M.W. Weatherburn. *Anal. Chem.*, **39**, 971 (1967).
[30] W. Zaborska, B. Krajska, Z. Olech. *J. Med. Chem.*, **19**, 65 (2004).
[31] D.D. Van Slyke, R.M. Archibald. *J. Biol. Chem.*, **154**, 623 (1944).
[32] M. Shakir, S. Parveen, N. Begum, Y. Azim. *Polyhedron*, **22**, 3181 (2003).
[33] M.H. Klingele, P.D.W. Boyd, B. Moubaraki, K.S. Murray, S. Brooker. *Eur. J. Inorg. Chem.*, **2006**, 573 (2006).
[34] M.X. Peng, C.G. Hong, C.K. Tan, J.C. Chen, M.L. Tong. *J. Chem. Crystallogr.*, **36**, 703 (2006).
[35] W.H.R. Shaw, D.N. Raval. *J. Am. Chem. Soc.*, **83**, 3184 (1961).
[36] C. Preininger, O.S. Wolfbeis. *Biosens. Bioelectron.*, **11**, 981 (1996).